The Formability of Austenitic Stainless Steels

S.F. Peterson, M.C. Mataya, and D.K. Matlock

This article reports the results of a study to determine the effects of austenite stability, with respect to the strain-induced transformation to martensite, on the formability of 300 series stainless steels. The effects were evaluated as a function of alloy content, deformation temperature, and deformation rate. Three stainless-steel alloys with different nickel contents were evaluated as commercially cold-rolled and annealed sheet products. Tensile tests were performed at temperatures between –60°C and +125°C and at strain rates from 0.00167 s^{-1} to 0.167 s^{-1}. The combined effects of strain, strain state, deformation-induced temperature changes, and strain rate are considered to explain the interrelationships between martensite formation and limit strains as observed in forming-limit diagrams.

INTRODUCTION

The formability of austenitic stainless steels is strongly dependent upon alloy composition, strain state, and strain path. These variables influence the ease and amount of martensite that is formed from the parent austenite phase. During deformation, martensite formation is enhanced by low strain rates, low temperatures, large deformations, and low amounts of alloying elements such as nickel, manganese, and nitrogen.

The effects of strain during standard tensile tests at room temperature on the transformation of austenite to martensite in metastable austenitic stainless steels has been evaluated by several investigators.[1-3] Angel[1] determined that the transformation is enhanced by high strains, low strain rates, low temperatures, and lower nickel contents. These results were verified by Hecker[2] and Huang et al.[3] The influence of martensite on the shape of tensile stress-strain curves has been evaluated by Ludwigson and Berger,[4] who developed a curve-fitting equation to describe the formation of martensite with strain, and by Olson and Cohen,[5] who developed an equation to describe the transformation kinetics based on martensite nucleation at shear-band intersections in austenite.

Recent studies predict the transformation of austenite to martensite in tension with the additional complexities of temperature, adiabatic heating, and strain states. Kumar and Singhal[6,7] used finite-element modeling to predict the amount of martensite formed in uniaxial tensile deformation of 304 stainless steel under both isothermal and adiabatic heating conditions. Their initial study,[6] based on the kinetic parameters of Olson and Cohen,[5] predicted that under adiabatic conditions, the center of a tensile bar would contain less martensite than the rest of the gage length. However, in a subsequent paper,[7] they modified their transformation parameters after experimentally determining that the martensite content is highest in the center of the tensile sample gage length.

In analyses similar to those applied to tensile deformation, the response of metastable stainless steel to complex strain paths in metal-forming operations has also been evaluated and modeled. Ramirez et al.[8] and Tsuta et al.[9] modeled the upsetting of a 304 stainless-steel cylinder. They modified the Ludwigson and Berger[4] curve fit to include temperature and predicted-strain partitioning between the austenite and martensite phases. Shinagawa et al.[10] modeled deep

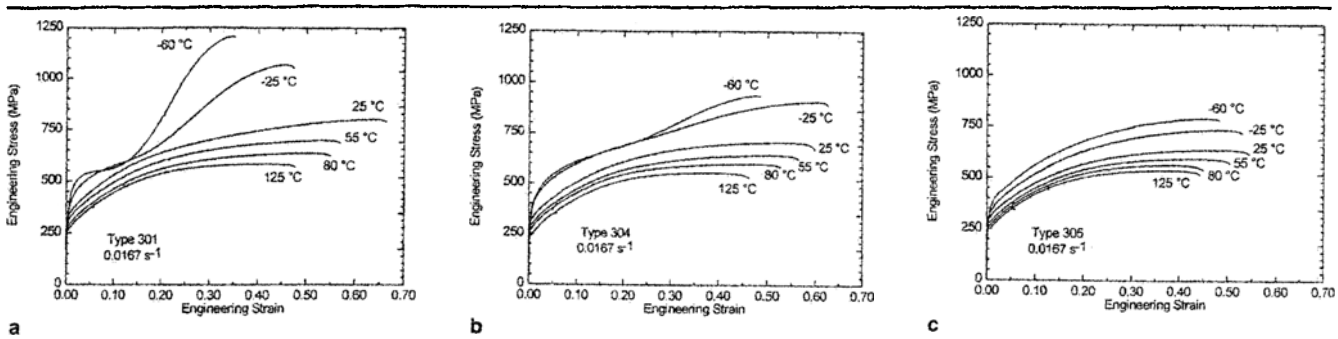

Figure 1. Engineering stress-strain curves for (a) 301, (b) 304, and (c) 305 tested between –60°C and 125°C at a strain rate of 0.0167 s^{-1}.

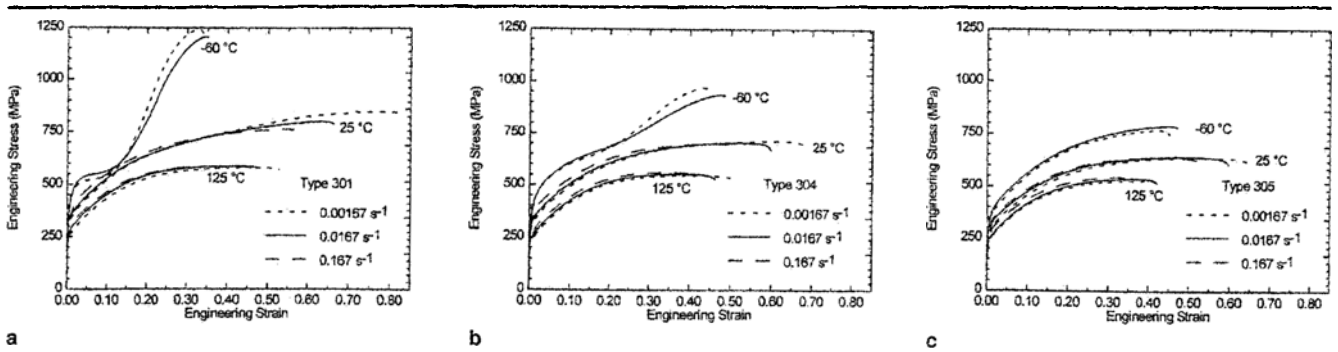

Figure 2. Engineering stress-strain curves for (a) 301, (b) 304, and (c) 305 tested at strain rates between 0.00167 s^{-1} and 0.167 s^{-1} at –60°C, 25°C, and 125°C.

drawing of 304 and 316 austenitic stainless steels using finite-element methods and included the effect of heating on transformation. Their analysis predicted failure locations in sheet deep drawn at different strain rates and temperatures.

The importance of strain path on martensite formation was modeled by Stringfellow et al.[11] in their analyses of plane-strain compression, simple compression, pure shear, uniaxial tension, and plane-strain tension. Their results, based on the kinetics equation of Olson and Cohen,[5] predicted that martensite formation was maximized in plane-strain tension.

The extent of austenite transformation to martensite has been evaluated

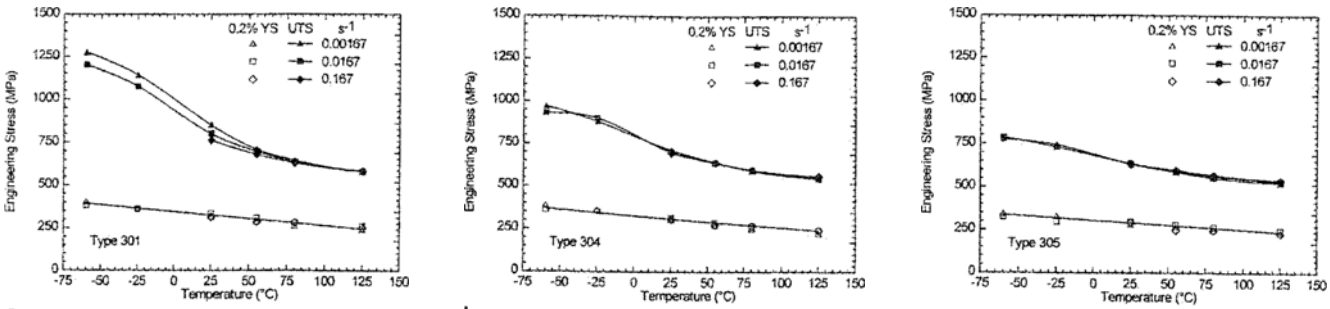

Figure 3. Ultimate tensile stress and 0.2% offset yield stress for (a) 301, (b) 304, and (c) 305 tested at temperatures between –60°C and 125°C and at strain rates between 0.00167 s^{-1} and 0.167 s^{-1}.

EXPERIMENTAL PROCEDURES

Three alloys, 301, 304, and 305, were received in the form of cold-rolled and annealed sheets. Compositions and sheet thicknesses of each alloy are given in Table 1.[16] Table 2 contains the martensite start, M_S, temperature (in °C) calculated from the equation of Eichelman and Hull[17] and M_{030}, the temperature (in °C) at which 50 percent of the austenite transforms to martensite at a true strain of 0.3 calculated from the equation of Angel.[1]

$$M_s = 41.7\,(14.6 - Cr) + 61.1\,(8.9 - Ni) + 33.3\,(1.33 - Mn) + 27.8\,(0.47 - Si) + 1666.7\,(0.068 - (C + N)) - 17.8 \quad (A)$$

$$M_{030} = 413 - 462\,(C + N) - 9.2\,(Si) - 8.1\,(Mn) - 13.7\,Cr - 9.5\,(Ni) - 18.5\,(Mo) \quad (B)$$

Alloying elements are in weight percent.

Uniaxial tension tests were performed at temperatures ranging between –60°C and 125°C and at strain rates between 0.00167 s^{-1} to 0.167 s^{-1}. ASTM standard E-8 tensile samples oriented parallel to the rolling direction were machined with a 50.8 mm gage length and a nominal width of 12.7 mm. Machined edges of the tensile samples were polished to eliminate any cold-worked or transformed regions. A pattern composed of 2.54 mm diameter circles was electrochemically etched[18] on the surface of each tensile sample.

All tensile testing was performed on a commercial floor model tensile machine. Tensile tests were performed on samples that were completely submerged in cooling or heating fluids—in an ethanol bath cooled by refrigerating coils for temperatures below 25°C and in an isothermal oil bath for temperatures at and above room temperature. During testing, length strains were measured by a submersible extensometer with a 51 mm gage length. Because this extensometer has a limited extension of 25 mm (50% engineering strain), tensile strains were extrapolated beyond 50% elongation. Each material was tested at six different temperatures (–60°C, –25°C, 25°C, 55°C, 80°C, and 125°C) and three different engineering strain rates (0.00167 s^{-1}, 0.0167 s^{-1}, and 0.167 s^{-1}).

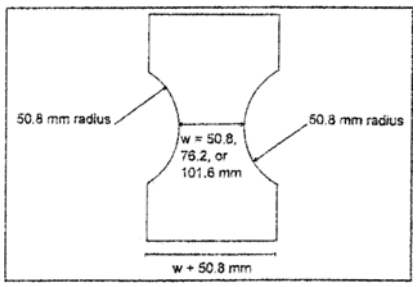

Figure A. Modified LDH test sample geometry.

A commercial ferrite meter calibrated against quantitative x-ray diffraction results was used to measure the volume fraction of martensite present in each tensile sample after deformation. For each tensile sample, the median and maximum volume-fraction values were based on 17 readings initially evenly spaced along the tensile gage length.

LDH tests with a 102 mm diameter spherical punch were performed at room temperature in air on each material on a laboratory system adapted to a commercial servohydraulic test frame.[19] For each material, samples 178 mm in length oriented parallel to the rolling direction were sheared to widths of 25 mm, 127 mm, 152 mm, and 178 mm. In addition, 102 mm wide strips of 305 stainless steel were sheared.

A grid pattern composed of 2.54 mm diameter circles was electrochemically etched onto the surface of each specimen. Test specimens with an hourglass or dog-bone shape (Figure A)[20] were substituted for the 51 mm, 76 mm, and 102 mm wide strips because of the tendency for the rectangular samples of these widths to fracture along the lockbead before the LDH was reached.

Two lubrication schemes were used for LDH testing. The first consisted of a spray lubricant applied to the side of the sample in contact with the punch. The second lubrication condition consisted of the spray lubricant in combination with a thin polyethylene sheet. The spray lubricant was applied to the test sample and both sides of the polyethylene sheet. For the former lubrication condition, one sample was deformed; for the latter, duplicate samples were deformed. Each LDH test sample was deformed at a punch rate of 0.212 mm/s to failure. The applied load and actuator displacement were measured during testing.

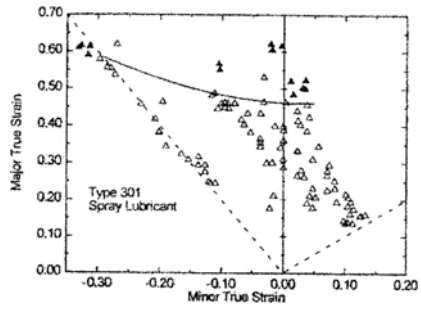

Figure B. An FLD for 301 tested at room temperature with a spray lubricant at an actuator speed of 0.212 mm/s. This diagram demonstrates how forming-limit curves were drawn.

Table 2. Calculated M_S and M_{030} Temperatures[1,17]

Alloy	M_S (°C)	M_{030} (°C)
301	–130	23
304	–240	–3.6
305	–273	–2.2

After testing, major and minor strains were measured with an image analyzer from grid circles along the LDH samples. Circles that were fractured or necked were classified as failed, whereas all other measured circles were designated safe. Thickness strains were calculated from the output of a commercial ultrasonic thickness gage, and volume fractions of martensite were measured with the ferrite meter. Forming-limit curves were determined for each lubrication condition by connecting the locus of points of the safe circles with the largest strains as shown in Figure B, which includes all of the experimental strain data for 301 stainless steel tested with the spray lubricant. Additional circles along the test sample were measured in order to provide measurements of the volume fraction of martensite versus von Mises effective strain.

Table 1. Sheet Thicknesses of Experimental Sheet Steels[16]

Alloy	C	Mn	P	S	Si	Cr	Mo	Ni	Cu	Cb	V	N	Nb	W	Thickness (mm)
301	0.096	1.85	0.024	0.0003	0.42	17.33	0.35	6.66	0.70	0.010	0.072	0.042	0.11	0.018	0.660
304	0.059	1.82	0.027	0.0007	0.42	18.50	0.50	8.07	0.46	0.017	0.087	0.068	0.067	0.021	0.635
305	0.032	1.00	0.024	0.0005	0.49	18.58	0.45	11.84	0.44	0.009	0.092	0.027	0.063	0.022	0.508

experimentally in several mechanical tests designed to evaluate the formability of sheet stainless steels. Hecker et al.[2] evaluated the response of 304 stainless steel to deformation in limiting-dome height (LDH) and Marciniak samples under a variety of strain paths. These results showed that balanced biaxial stretching produced the most martensite for a given amount of von Mises effective strain. The importance of strain gradients on deformation during the stretch forming of 304 stainless steel was evaluated by Coubrough et al.[12] in an analysis of LDH samples of different widths. Strain gradients were correlated with direct measurements of the temperature gradients induced during deformation. Test conditions that led to significant temperature increases limited martensite formation with strain and, correspondingly, limited punch heights at failure. These results emphasized the complex relationship between martensite formation and formability.

To date, limited forming-limit diagrams (FLD) for metastable austenitic stainless steels have been published,[2,13-15] and most of the previous results have been obtained in air on 304 stainless steel with few results regarding other stainless-steel alloys. In addition, while it has been shown for specific loading conditions such as uniaxial tension[1-4] that ductility depends on both the extent of martensite formation and the strain at which martensite forms, previous analyses that have led to published FLDs have not correlated the extent of martensite formation with strain limits on the FLDs.

Previous investigations have shown the importance of strain rate, temperature, adiabatic heating, etc. on the mechanical properties of austenitic stainless steels. However, these investigations have limitations in that most of the individual studies only involve one alloy, one test method, and one strain state. The purpose of this work was to generate traditional FLDs for three alloys with different austenite stabilities and to provide modified FLDs that incorporate transformation-induced plasticity. These new FLDs will provide an enhanced understanding of the effect of martensite formation on formability. Additional factors, such as the relationships between strain and temperature and strain and temperature gradients, are incorporated into these modified FLDs.

TENSILE TESTING

The effects of alloy composition and temperature on engineering stress-strain curves at a strain rate of 0.0167 s^{-1} are shown in Figure 1. The effects of composition and strain rate on stress-strain curves are shown for selected temperatures in Figure 2.

At low temperatures, both 301 and 304 stainless steel exhibit sigmoidal stress-strain curves characteristic of austenitic materials that form to martensite with strain.[2,3,5] However, for 301 and 304 at higher temperatures and 305 at all temperatures, conventional parabolic stress-strain curves that are characteristic of stable austenitic alloys or alloys that transform to martensite only at strains within the post-uniform deformation region are observed.[2-4]

From the stress-strain curves in Figures 1 and 2, values of ultimate tensile strength (UTS), 0.2% yield strength, and uniform and total elongation values were reduced (Figures 3 and 4). For all three alloys, the UTS decreased with an increase in temperature and was essentially independent of strain rate, except for 301 at low temperatures, where UTS increased with a decrease in strain rate. For all three alloys, the 0.2% offset yield stress decreased slightly with an increase in temperature. Uniform and total elongations exhibit maxima with an increase in temperature.

The volume fraction of martensite that formed within the uniformly strained sections of failed tensile samples is summarized in Figure 5 for each material. For all alloys, the volume-fraction martensite decreased with an increase in temperature. At low temperature, the amount of martensite that formed was significantly higher in 301. Figure 5 shows that 305 always has significantly lower volume-fraction martensite than 304. This contradicts the M_{D30} temperatures calculated for each alloy in Table 2 of the sidebar, which indicate that 304 and 305 should have the same degree of stability against transformation to martensite. The differences in composition between 304 and 305 are the manganese, nickel, nitrogen, and carbon contents. The difference in the austenite stability against strain in 304 and 305 may indicate that the M_{D30} calculation may not be as strong a function of these elements as Equation B in the sidebar suggests.

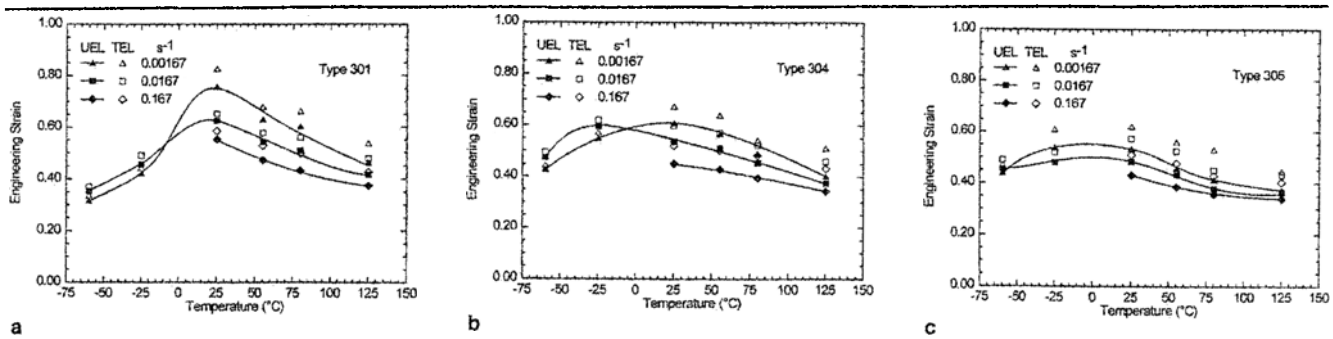

Figure 4. Uniform and total strains for (a) 301, (b) 304, and (c) 305 tested at temperatures between –60°C and 125°C and at strain rates between 0.00167 s^{-1} and 0.167 s^{-1}.

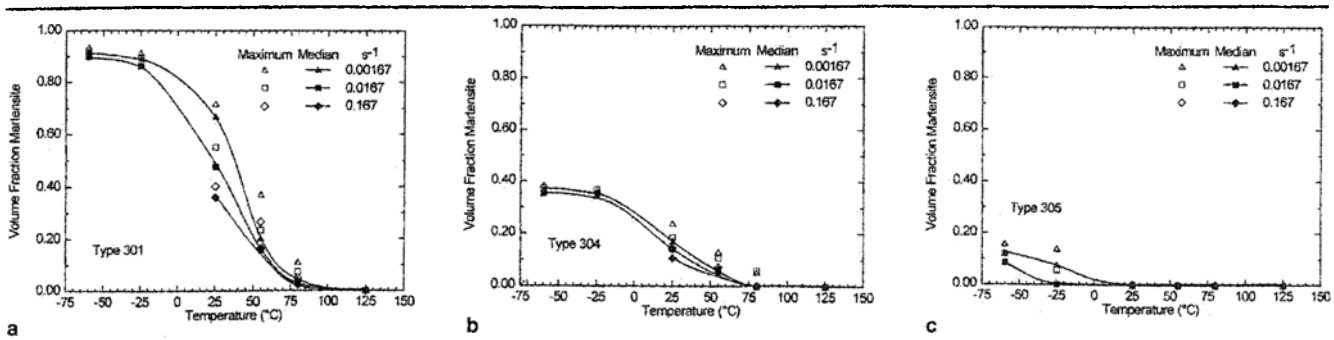

Figure 5. The volume fraction of martensite formed in (a) 301, (b) 304, and (c) 305 tested at temperatures between –60°C and 125°C and at strain rates between 0.00167 s^{-1} and 0.167 s^{-1}. Median measurements are from the uniform strain region of the tensile sample after failure.

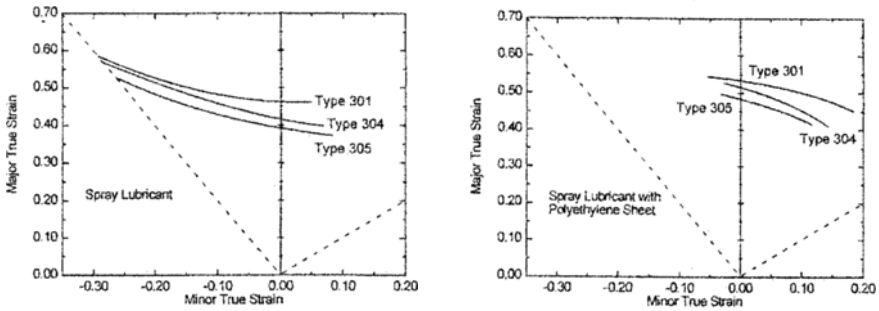

Figure 6. Forming-limit curves for 301, 304, and 305 that were tested at room temperature at an actuator speed of 0.212 mm/s with (a) spray lubricant and (b) with a spray lubricant plus a polyethylene sheet.

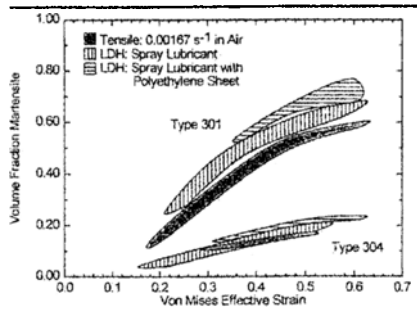

Figure 7. The volume fraction of martensite formed in 301 and 304 versus von Mises effective strain under different test methods and conditions.

At 125°C, a temperature where austenite is stable for all alloys, differences in UTS between each alloy are small. As the test temperature is decreased, differences become more apparent. The alloy with the least stable microstructure, 301, developed much higher strength than 304 and 305 at temperatures and strain rates where martensite formed in significant quantities. It also showed higher strength than 305 when martensite was formed. At the test temperatures utilized, differences in yield strength between each alloy were not significant. These small differences in yield strength and the observation that yield strength continuously decreases with increases in temperature indicate that all martensite formed was strain-induced.[5] Between the M_S and M_D temperatures, stress-assisted martensite would form, and the yield strength would appear to decrease with a decrease in test temperature due to the higher specific volume of martensite.

Alloy composition and temperature also have an impact on uniform elongation (Figure 4). Temperature affects the amount of martensite formed in each alloy at a specific strain. As shown in Figure 5, 301 is completely stable above 80°C, whereas, 304 and 305 are stable above 55°C and –25°C, respectively. The formation of martensite has the ability to significantly alter the shape of stress-strain curves (Figure 1). When the austenite is stable, a typical stress-strain curve for a face-centered cubic material is acquired. At temperatures where martensite forms during uniform deformation, the stress-strain curve initially follows the pure austenite curve and then deviates upward as the higher strength martensite is formed.

At temperatures where austenite is stable, differences in uniform elongation between alloys are reduced. However, in the 25°C to 55°C temperature range, martensite forms in 301 and 304 at high strains within the uniform deformation region, while no martensite forms in 305. The effect of martensite formation in this temperature range is to increase the ductility of 301 and 304. In the –60°C to –25°C temperature range, martensite forms at low strains to produce significant strength increases in both 301 and 304, and as a result, the ductility of these alloys decreases significantly, while the ductility of 305 does not decrease as severely. These characteristics can be seen by comparing the stress-strain curves for 301 and 305 at –60°C. Type 305, which forms very little martensite at –60°C, displays a stress-strain curve typical of pure austenite; 301 shows a significant increase in strength at about 0.15 engineering strain. The stress-strain curve for 301 at –60°C actually drops below the curve obtained at –25°C. This is a result of dynamic softening and a volume increase from the new martensite phase.

Strain rate also has a significant effect on the engineering stress-strain curve as shown in Figure 2 for each alloy at –60°C, 25°C, and 125°C. When the austenite is stable, increases in strain rate have little effect on the UTS, but decrease ductility. When the austenite is metastable, higher strain rates will suppress the formation of martensite and decrease the UTS. The effect of strain rate on ductility depends on the transformation kinetics. At low temperatures where martensite forms at low strains, ductility will be enhanced. At higher temperatures, transformation-induced plasticity will be reduced or eliminated.

FORMING-LIMIT DIAGRAMS

Figure 6 shows forming-limit curves for each material under two lubrication conditions: spray lubricant and polyethylene in combination with the spray lubricant. The data (e.g., Figure B) are omitted for clarity, and a complete summary of actual strain measurements can be found elsewhere.[21] In each figure, the ends of the solid lines represent the extent of minor true strains observed for the various sample widths. With the spray lubricant, very little of the stretching side (minor strain > 0) of the FLD was exploited. Increasing lubricity by adding one thin piece of polyethylene moved the forming-limit curves to increased biaxiality. In areas of formability where the two lubrication conditions overlap, increased lubrication raised the limiting strains for all alloys. Increased lubrication raises the curves because strain gradients within individual grid circles are lower as the material is able to better distribute strain. For polyethylene in combination with the spray lubricant, forming-limit curves were not defined on the drawing side (minor strain < 0) because no narrow samples were tested. For the lubrication conditions, temperature, and punch rate used, 301 had the highest forming-limit curve, followed by 304. These higher forming limits are attributed to the transformation-induced plasticity that suppresses neck formation. As the material is deformed, austenite transforms to martensite, and the resulting volume expansion helps the material to resist thinning.

It should be noted that the data shown

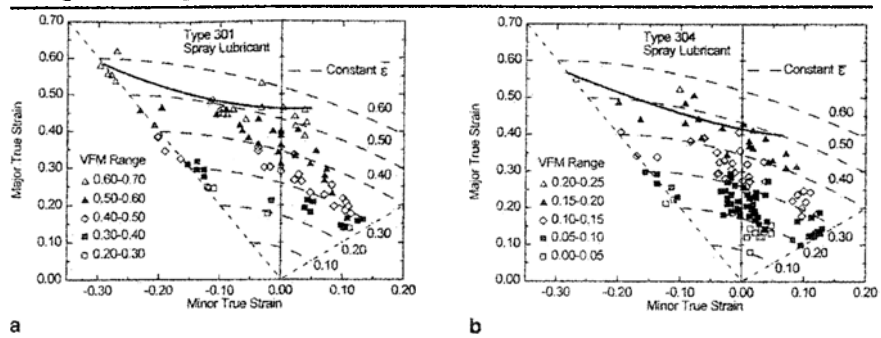

Figure 8. Modified FLDs for (a) 301 and (b) 304 tested at room temperature at an actuator speed of 0.212 mm/s with a spray lubricant. FLDs show the relationship of volume fraction martensite with von Mises effective strain and the forming limit curve.

in Figure 6b indicate that the minimum major strain lies to the right of the plane strain value, an observation which is counter to most FLDs for materials with stable microstructures. This apparent shift in the location of the strain minima may reflect complex interactions between lubrication, which modifies strain gradients, and the location of the neck. For each test sample with spray lubrication, failure occurred in the ligament region with the major strain of the fractured circles oriented parallel to the rolling direction. Increasing lubricity by adding a thin polyethylene sheet moved the failure location for test samples of each material that were 127 mm and 152 mm wide toward the pole region. For 127 mm and 152 mm wide samples, the failure location moved approximately 3 mm and 1.5 (1 grid and 0.5 grid circles) toward the pole. For the 178 mm wide (fully constrained) samples, the location of the failed circles did not move significantly, but the orientation of the major strain of the failed circles became perpendicular of the rolling direction. The apparent anomaly in Figure 6b must be investigated further.

VOLUME FRACTION MARTENSITE VS. VON MISES EFFECTIVE STRAIN

Figure 7 shows the relationship between volume-fraction martensite and von Mises effective strain for 301 and 304 under different test methods. The tests included in Figure 7 are room-temperature tensile samples deformed in air at 0.00167 s^{-1} and LDH tests under the two lubrication conditions described previously. Von Mises effective strain is given by[22]

$$\bar{\varepsilon} = \sqrt{\frac{2}{3}\left(\varepsilon_{major}^2 + \varepsilon_{minor}^2 + \varepsilon_{thickness}^2\right)} \quad (1)$$

where ε_{major}, ε_{minor}, and $\varepsilon_{thickness}$ denote true major, minor, and thickness strains in a deformed sample. In Figure 7, the data points[21] are omitted for clarity and data bands are presented for comparison.

For all three data sets for each material, the volume fraction of martensite increased with effective strain. At a given amount of effective strain, more martensite is formed during LDH testing than tensile testing for both 301 and 304. This can be attributed to martensite formation being more favorable thermodynamically in the stretching side of the forming-limit curve than the drawing side.[23] In the LDH test, the test material can be completely constrained, whereas in a tensile sample, material can draw in from the sides. Figure 7 also shows that increased lubrication in LDH testing will produce more martensite for a given amount of effective strain. This may be due to reduced strain gradients along the samples deformed with higher lubrication. Considering work from Coubrough et al.,[12] it is believed that this phenomena is not attributable to higher adiabatic heating in less well-lubricated samples. It should be noted that the correlation that is shown in Figure 7 is for samples that are subjected to a single strain path.

The direct relationship between forming limits and the extent of martensite formation during deformation is illustrated in Figure 8. This figure includes the forming limit curves from Figure 6a for 301 (Figure 8a) and 304 (Figure 8b) combined with maps of the extent of martensite formation in strain space for each alloy. To obtain the martensite data in Figure 8, each circle used to evaluate the safe range of the FLD (e.g., the open triangles in Figure B) was identified, and the martensite volume fraction was measured within the circle as the diameter sampled by the ferrite meter probe was essentially the same size as the grid circle. Martensite volume-fraction ranges were then identified (e.g., 0.0–0.05, 0.05–0.10, etc. for 304 and 0.2–0.3, 0.3–0.4, etc. for 301). Each range was assigned a symbol and plotted at the appropriate major and minor strains. Also superimposed on the figures are calculated lines of constant von Mises effective strain according to Equation 1. The constant martensite volume fraction bands are shown to essentially follow constant von Mises effective strain lines, and the limit strains that define the forming limit are contained within one constant martensite volume fraction band.

CONCLUSIONS

Figure 8 presents a new method of incorporating the microstructural changes that occur with strain in metastable austenitic stainless steels in standard FLDs. From the tensile data presented, it is clear that the magnitudes of the constant martensite volume fraction bands will depend sensitively on temperature, strain rate, and alloy content. To properly utilize FLDs for metastable austenitic stainless steels, the effects of deformation variables on microstructural changes that occur with strain must be evaluated. The results presented here have illustrated one method of incorporating strain limits and microstructural data. To properly optimize the use of metastable austenitic stainless steels, additional experimental evaluations and analytical analyses are required.

ACKNOWLEDGEMENTS

The authors acknowledge the support of the Advanced Steel Processing and Products Research Center, a National Science Foundation industry-university cooperative research center at the Colorado School of Mines.

References

1. T. Angel, "Formation of Martensite in Austenitic Stainless Steels. Effects of Deformation, Temperature, and Composition," *J. of the ISI*, 5 (1954), pp. 165–174.
2. S.S. Hecker et al., "Effects of Strain State and Strain Rate on Deformation-Induced Transformation in 304 Stainless Steel: Part I. Magnetic Measurements and Mechanical Behavior," *Met. Trans. A*, 13A (1982), pp. 619–626.
3. G.L. Huang, D.K. Matlock, and G. Krauss, "Martensite Formation, Strain Rate Sensitivity, and Deformation Behavior of Type 304 Stainless Steel Sheet," *Met. Trans. A*, 20A (1989), pp. 1239–1246.
4. D.C. Ludwigson and J.A. Berger, "Plastic Behaviour of Metastable Austenitic Stainless Steels," *J. of the ISI*, 1 (1969), pp. 63–69.
5. G.B. Olson and M. Cohen, "Kinetics of Strain-Induced Martensitic Nucleation," *Met. Trans. A*, 6A (1975), pp. 791–795.
6. A. Kumar and L.K. Singhal, "Effect of Temperature and Strain Distribution on Martensitic Transformation during Uniaxial Testing of AISI-304 Stainless Steel," *Met. Trans. A*, 19A (1988), pp. 1021–1026.
7. A. Kumar and L.K. Singhal, "Effect of Strain Rate on Martensitic Transformation during Uniaxial Testing of AISI-304 Stainless Steel," *Met. Trans. A*, 20A (1989), pp. 2857–2859.
8. J.A.C. Ramirez et al., "Flow Stress and Phase Transformation Analyses in the Austenitic Stainless Steel under Cold Working. Part 1, Phase Transformation Characteristics and Constitutive Formulation by Energetic Criterion," *JSME International Journal*, 35 (1) (1992), pp. 201–209.
9. T. Tsuta and J.A. Cortes R., "Flow Stress and Phase Transformation Analyses in Austenitic Stainless Steel under Cold Working. Part 2, Incremental Theory Under Multiaxial Stress State by the Finite-Element Method," *JSME International Journal*, 36 (1) (1993), pp. 63–72.
10. K. Shinagawa, K. Mori, and K. Osakada, "Finite Element Simulation of Deep Drawing of Stainless Steel Sheet with Deformation-Induced Transformation," *J. of Mat. Proc. Tech.*, 27 (1991), pp. 301–310.
11. R.G. Stringfellow, D.M. Parks, and G.B. Olson, "A Constitutive Model for Transformation Plasticity Accompanying Strain-Induced Martensitic Transformations in Metastable Austenitic Steels," *Acta Metallurgica et Materialia*, 40 (7) (1992), pp. 1703–1716.
12. G.J. Coubrough, D.K. Matlock, and C.J. Van Tyne, *Formability of Type 304 Stainless Steel Sheet*, SAE technical paper 930814 (1993), pp. 279–289.
13. A. Graf and W.F. Hosford, "Calculations of Forming Limit Diagrams," *Met. Trans. A*, 21A (1990), pp. 87–94.
14. K.J. Blom, "Press Formability of Stainless Steels," *Stainless Steel '77* (London: Amax, 1977), pp. 213–216.
15. A.S. Korhonen, "Work-Hardening and Formability of Austenitic Stainless Steel Sheets," *Sheet Metal Industries*, 5 (1978), pp. 598–606.
16. I.A. Franson, Allegheny Ludlum Technical Center, private communication, May 1995.
17. A.H. Eichelman and F.C. Hull, "The Effect of Composition on the Temperature of Spontaneous Transformation of Austenite to Martensite in 18-8 Type Stainless Steel," *Transactions of the ASM*, 45 (1953), pp. 77–104.
18. Lectroetch Company, *Electrochemical Marking Manual* (East Cleveland, OH: Lectroetch Co., 1971), pp. 18–19.
19. D.A. Burford, "Frictional and Geometric Effects in Punch-Stretch Sheet Metal Formability Testing," Ph.D. thesis, Colorado School of Mines (1987).
20. E.P. Cooke, R.P. Foley, and D.K. Matlock, *Formability of Ferritic Stainless Steel Sheet*, ASPPRC research report MT-SRC-095-020 (Colorado School of Mines: ASPPRC, September 1, 1995).
21. S.F. Peterson, "Formability of Austenitic Stainless Steels," M.S. thesis, Colorado School of Mines (1996).
22. G.E. Dieter, *Mechanical Metallurgy* (New York, NY: McGraw-Hill, 1986), pp. 88–89.
23. G.B. Olson and M. Cohen, "Stress-Assisted Isothermal Martensitic Transformation: Application to TRIP Steels," *Met. Trans. A*, 13A (1982), pp. 1907–1914.

ABOUT THE AUTHORS

S.F. Peterson earned his M.S. in metallurgical and materials engineering from the Colorado School of Mines in 1997. He is currently an engineer at Case Corporation.

M.C. Mataya earned his Ph.D in metallurgy and materials science from Marquette University in 1976. He is currently an engineer at the Rocky Flats Technology Site.

D.K. Matlock earned his Ph.D. in materials science and engineering from Stanford University in 1972. He is currently a professor at the Colorado School of Mines. Dr. Matlock is also a member of TMS.

For more information, contact S.F. Peterson, Case Corporation, Technology Center, 7 S. 600 County Line Road, Burr Ridge, Illinois 60521, (630) 887-5472.